A unified constitutive model for variably saturated soils including hydraulic and mechanical hystereses

Zargarbashi S., Khalili N., and Habte M.A
School of Civil and Environmental Engineering, University of New South Wales, Sydney, NSW, Australia

ABSTRACT
A fully coupled constitutive model is presented for stress-strain behaviour of unsaturated soils. The elastic-plastic behaviour due to loading and unloading is captured using the bounding surface plasticity. The hydraulic hysteresis is accounted for through the soil water characteristic curve. Attention is also given to the interrelations between the effective stress and wetting and drying paths, and the shift in the soil water characteristic curve with the matrix deformation. A single set of material parameters is introduced for the characterization of the coupled constitutive model. Comparisons are made between the simulation results and experimental data from the literature highlighting capabilities of the model.

RÉSUMÉ
Un modèle constitutif et entièrement couplé est présenté pour le comportement contrainte-déformation des sols non-saturés. Le comportement élastique-plastique à cause de chargement et de déchargement est capturé à l'aide de la plasticité de limitant surface. L'hystérésis hydraulique est représentée par la courbe de caractéristique de l'eau du sol. L'attention est également accordée à l'interaction entre la contrainte efficace et l'humidification et des chemins de séchage, et le changement de la courbe de caractéristique d'eau de sol avec la matrice de déformation. Un ensemble de paramètres de matériel est introduit pour la caractérisation du couplage modèle constitutif. Les comparaisons sont faites entre les résultats de la simulation et les données expérimentales de la littérature mettant en évidence les capacités du modèle.

1 INTRODUCTION

Interrelation of hydraulic and mechanical behaviour in unsaturated soils is a subject of great interest in geotechnical engineering practice. The plastic volumetric strain affects the soil water characteristics curve and causes a change in the degree of saturation. Wetting and drying cycle, on the other hand, increases the stiffness (Gallipoli et al. 2003 and Wheeler et al. 2003) and causes irreversible volumetric strain (Alonso et al., 1995). Indeed, the description of the hydro-mechanical behaviour of unsaturated soils in a multiphase setting, and the identification of the influencing internal and external mechanisms has been a key area of research in modern geomechanics.

Several constitutive models have been proposed over the past few years. Among the notable contributions have included the work of Vaunat et al (2000), Jommi (2000), Buisson and Wheeler (2000), Wheeler et al (2003), Gallipoli et al (2003), as well as Tamagnini R (2004). Vaunat et al (2000) were perhaps first to incorporate the effect of hydraulic hysteresis into mechanical modelling of unsaturated soils. They used the Basic Barcelona Model as the plasticity platform and included two yield surfaces to capture irreversible changes in water content during drying and wetting. Wheeler and his colleagues adopted an effective stress approach and presented a coupled hysteretic hydro-mechanical model for isotropic loading. Later Wheeler's model was extended to deviatoric loading and casting into a classical theory of elasto-plasticity, a more general model of hydraulic hysteresis was also proposed, which resulted in variations to this model (Sun et al (2007a, b)).

The focus in the above contributions has however been the constitutive modelling of the solid skeleton and the hysteresis arising from the soil water characteristic curve. However, there are no models of unsaturated soils that take into account both the hydraulic and the mechanical hystereses in the constitutive modelling of unsaturated soils.

The objective in this paper is to present a more complete treatment of stress-strain modelling in variably saturated soils. The work is an extension of the theoretical developments of Habte and Khalili (2006) to include mechanical as well as hydraulic hysteresis. The essential aspects presented include: the effective stress principle and determination of effective stress parameters; the effective stress along wetting and drying paths; bounding surface elastic-plastic constitutive model to describe the deformation behaviour and mechanical hysteresis. All model parameters are identified in terms of measurable physical entities. Simulation results and comparisons with experimental data are presented to demonstrate the application of the model.

Throughout this paper, sign convention of continuum mechanics is adopted; Compressive stresses and strains are taken as negative. However, the mean normal stress and the volumetric strain (p and ε_v) are defined as $p = -\frac{1}{3}\boldsymbol{\delta}^{\mathrm{T}}\boldsymbol{\sigma}$ and $\varepsilon_v = -\boldsymbol{\delta}^{\mathrm{T}}\boldsymbol{\varepsilon}$ so that they are positive in compression following the soil mechanics convention. Similarly, pore water pressure (p_w) and pore air pressure

(p_a) are taken as positive in compression. Compact matrix-vector notation is used throughout. Bold face letters indicate matrices and vectors. $\nabla(\cdot) = \partial(\cdot)/\partial x$ is the spatial gradient and $\mathrm{div}(\cdot) = \nabla\cdot(\cdot)$ is the divergence operator and the identity vector is defined as $\boldsymbol{\delta} = \{1,1,1,0,0,0\}^{\mathrm{T}}$.

2 BASIC CONCEPT

2.1 Effective stress

The effective stress concept is undoubtedly a powerful tool for quantitative assessment of response in saturated and unsaturated soils, and plays a central role in the present formulation. It is used to cast the elastic and the elasto-plastic constitutive equations of the solid skeleton linking a change in stress to straining or any other relevant quantity of the solid skeleton (Khalili et al, 2005). It is also used as a platform for coupling the deformation of the solid skeleton to the volume change of the water and air constituents.

The effective stress for unsaturated soils was first expressed as (Bishop, 1959; Bishop and Blight, 1963)

$$\boldsymbol{\sigma}' = \boldsymbol{\sigma}_{net} - \chi s \boldsymbol{\delta} \qquad [1]$$

where $\boldsymbol{\sigma}_{net} = \boldsymbol{\sigma} + p_a \boldsymbol{\delta}$ is the net stress and $s \equiv p_a - p_w$ is the matric suction. Since elasto-plastic constitutive relations are highly non-linear, they are generally expressed using incremental equations. Accordingly, such equations require an equivalent form of the effective stress equation in an incremental format. The incremental form of the effective stress equation is obtained through a simple differentiation of [1] as

$$\dot{\boldsymbol{\sigma}}' = \dot{\boldsymbol{\sigma}}_{net} - \psi \dot{s} \boldsymbol{\delta} \qquad [2]$$

where a superimposed dot indicates the rate of change, $\dot{\boldsymbol{\sigma}}_{net} = \dot{\boldsymbol{\sigma}} + \dot{p}_a \boldsymbol{\delta}$ is the incremental net stress, $\dot{s} = \dot{p}_a - \dot{p}_w$ is the incremental suction, $\psi = d(\chi s)/ds$ is the incremental effective stress parameter.

2.2 Effective stress parameter

The effective stress parameter, χ, describes the contribution of suction to effective stress. It may also be regarded as the scaling factor averaging matric suction from the pore-scale level to a macroscopic level over the representative elementary volume. This parameter is strongly dependent on the soil structure and its determination is crucial for a successful application of effective stress based constitutive models to soil engineering problems. Earlier definitions of the effective stress parameter assumed direct correlation with the degree of saturation, S_r (Bishop, 1959; Bishop and Blight, 1963). They provided a geometrical interpretation of the effective stress parameter; however no unique relationship could be find between the degree of saturation and the effective stress parameter (Bishop and Donald, 1961). From thermodynamic considerations, Laloui et al (2003) stated that χ should be expressed in terms of the aerial fractions of the constituents rather than the volumetric fractions. They further added that χ is related to, but not equal to, the degree of saturation and is a function of porosity and the pore air and pore water pressures. Similarly, Hassanizadeh and Gray (1990), Houlsby (1997), Muraleeharan and Wei (1999) showed that ignoring the work of air-water interface the effective stress parameter may be taken as the degree of saturation. In recent years, several investigators have advocated the use of the degree of saturation as the effective stress parameter. However, the overwhelming experimental evidence, gathered since 1960's, is against the use of degree of saturation as the effective stress parameter (Zerhouni, 1991). In this formulation, the approach proposed by Khalili and Khabbaz (1998) and Khalili et al (2004) is adopted. In this approach, the effective stress parameter is linked to the soil structure through an experimentally obtained correlation between soil suction and the effective stress parameter. After analysing shear strength data using a range of soil types, Khalili and Khabbaz (1998) obtained a unique relationship for the effective stress parameter χ in terms of the suction ratio s/s_e that was later extended by Khalili et al. (2004). They established the following correlation

$$\chi = \begin{bmatrix} 1 & for \dfrac{s}{s_e} \le 1 \\ (\dfrac{s}{s_e})^{-0.55} & for 1 < \dfrac{s}{s_e} < 25 \\ 25^{0.45}(\dfrac{s}{s_e})^{-1} & for \dfrac{s}{s_e} > 25 \end{bmatrix} \qquad [3]$$

where s_e is the suction value marking the transition between saturated and unsaturated states. For the main wetting path $s_e = s_{ex}$, and for the main drying path $s_e = s_{ae}$, in which s_{ex} is the air expulsion value and s_{ae} is the air entry value. For suction reversals, Khalili and Zargarbashi (2009), by conducting detailed drying and wetting tests on several soil samples, showed that upon suction reversal from drying to wetting, χ decreases with decreasing suction until it reaches the main wetting path, from where it increases with further reductions in suction. Based on their observation, they proposed a simple model for hysteresis of the effective stress parameter in drying-wetting cycle with specific attention to variation of this parameter in transition from drying to wetting and vice versa (Figure 1).

The observed reduction in the value of χ upon suction reversal is thought to be due to the change in contact angle between the air-water interface and the solid grains which changes from receding to that of advancing during the suction reversal process (Khalili and Zargarbashi, 2009). Both s_{ex} and s_{ae} are *a priori* a function of the specific volume (density), $v = 1 + e$, where e is the void ratio. This leads to a shift to the right of the effective stress parameter curve with increasing density, (Figure 1).

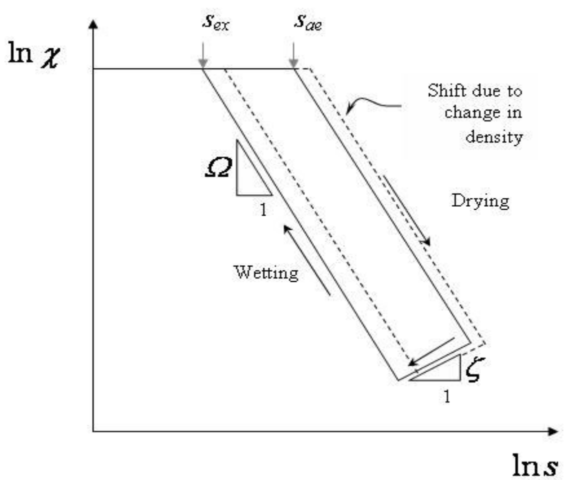

Figure 1. Evolution of effective stress parameter with hydraulic hystresis and with change in density

3 UNIFIED BOUNDING SURFACE PLASTICITY MODEL

The elastic-plastic deformation behaviour is captured through the bounding surface plasticity framework. In this approach, plastic deformation occurs when the stress state lies on or within the bounding surface. This is achieved by defining the hardening modulus h as a decreasing function of the distance between the stress point, $\boldsymbol{\sigma}'$, and an "image point" on the bounding surface. The image point is selected using a mapping rule such that the normals to the loading surface at $\boldsymbol{\sigma}'$, and to the bounding surface at the image point, $\bar{\boldsymbol{\sigma}}$, are the same. The essential elements of the bounding surface plasticity are (Dafalias and Herrmann, 1980): a bounding surface separating admissible from inadmissible states of stress; a loading surface on which the current stress state lies; a plastic potential describing the mode and component magnitudes of plastic deformation; and the hardening rule, controlling the movement of the current stress state towards the image point on the bounding surface as well as the size and locations of the loading and bounding surfaces. In the model presented, the material behaviour is assumed isotropic and rate independent in both elastic and elastic-plastic responses. The plasticity model is formulated using effective stress in the $p' - q$ plane, $p' = -\frac{1}{3}\left(\boldsymbol{\delta}^{\mathrm{T}}\boldsymbol{\sigma}'\right)$ is the mean normal effective stress and $q = \sqrt{3J_2}$ is the deviatoric stress. $J_2 = \frac{1}{2}\left(\mathbf{s}^{\mathrm{T}}\mathbf{s}\right)$ is the second invariant of the deviator stress vector, $\mathbf{s} = \boldsymbol{\sigma}' + p'\boldsymbol{\delta}$. The corresponding work conjugates strains are volumetric strain $\varepsilon_v = -\boldsymbol{\delta}^{\mathrm{T}}\boldsymbol{\varepsilon}$ and deviatoric strain $\varepsilon_q = \sqrt{\frac{2}{3}\left[\left(\boldsymbol{\varepsilon} + \frac{1}{3}\varepsilon_v\boldsymbol{\delta}\right)^{\mathrm{T}}\left(\boldsymbol{\varepsilon} + \frac{1}{3}\varepsilon_v\boldsymbol{\delta}\right)\right]}$.

3.1 Bounding surface

Similar to the yield surface in the conventional plasticity, the bounding surface is selected experimentally. Various stress paths may be chosen for this purpose. For materials where the contribution of elasticity to volume change is negligible, the undrained response in the effective stress plane follows closely the bounding surface. Within this context, the function (F) below was found to best fit the experimental data (Khalili et al., 2005)

$$F(\bar{p}', \bar{q}, \bar{p}'_c) = \bar{q} - M_{cs}\bar{p}'\left[\frac{\ln\left(\bar{p}'_c / \bar{p}'\right)}{\ln R}\right]^{1/N} = 0 \qquad [4]$$

where the superimposed bar denotes stress conditions on the bounding surface, M_{cs} is the slope of the critical state line (CSL) in the $q \sim p'$ plane. The parameter $\bar{p}'_c$ controls the size of F and is a function of suction and plastic volumetric strain. The material constant R represents the ratio between $\bar{p}'_c$ and the value of $\bar{p}'$ at the intercept of F with the critical state line in the $q \sim p'$ plane. The material constant N controls the curvature. M_{cs} is defined as

$$M_{cs} = \left(\frac{q}{p'}\right)_{cs} = \frac{6\sin\phi'_{cs}}{3\tilde{t} - \sin\phi'_{cs}} \qquad [5]$$

where ϕ'_{cs} is the constant volume, effective friction angle, $\tilde{t} = +1$ for compressive loading ($q > 0$), $\tilde{t} = -1$ for extensive loading ($q < 0$) and the subscript cs denotes conditions at the critical state. In the three dimensional general stress space, the slope of the critical state line

(M_{cs}) is expressed as a function of the Lode angle θ. The Lode angle is defined by

$$\theta = \frac{1}{3}\sin^{-1}\left[-\frac{3\sqrt{3}}{2}\frac{J_3}{\sqrt{(J_2)^3}}\right] \qquad [6]$$

where J_2 and J_3 are the second and third invariants of the deviator stress vector. The Lode angle ranges from $\theta = -\pi/6$ for triaxial extension to $\theta = +\pi/6$ for triaxial compression. Lode angle dependency of M_{cs} determines the shape of the yield and failure surfaces in the deviatoric (π) plane of the principal stress space. A convenient expression for the variation of M_{cs} with θ is

$$M_{cs}(\theta) = M_{\max}\left(\frac{2\alpha^4}{1+\alpha^4-(1-\alpha^4)\sin 3\theta}\right)^{\frac{1}{4}} \qquad [7]$$

where α is given by

$$\alpha = \frac{M_{\min}}{M_{\max}} = \frac{3-\sin\phi'_{cs}}{3+\sin\phi'_{cs}} \qquad [8]$$

M_{max} is the value of M_{cs} for triaxial compression and M_{min} is the value of M_{cs} for triaxial extension.

3.2 Loading surface

The conventional definition that $\boldsymbol{\sigma}'$ is always located on a loading surface is applied here. The loading surface adopted is of the same shape and is homologous to the bounding surfaces about the centre of homology. For first time loading, the centre of homology is at the origin of stresses in $q \sim p'$ plane. For cyclic loading, the centre of homology moves to the last point of stress reversal and the maximum loading surface through the point of stress reversal serves as a local bounding surface for the loading surfaces within the maximum loading surface (Figure 2). To maintain similarity with the bounding surface, the loading surfaces undergo kinematic hardening during loading and unloading such that they are tangent to the maximum loading surface at the centre of homology. The image point for cyclic loading is located sequentially by projecting the stress point onto a series of intermediate image points on successive local bounding surfaces passing through each point of stress reversal.

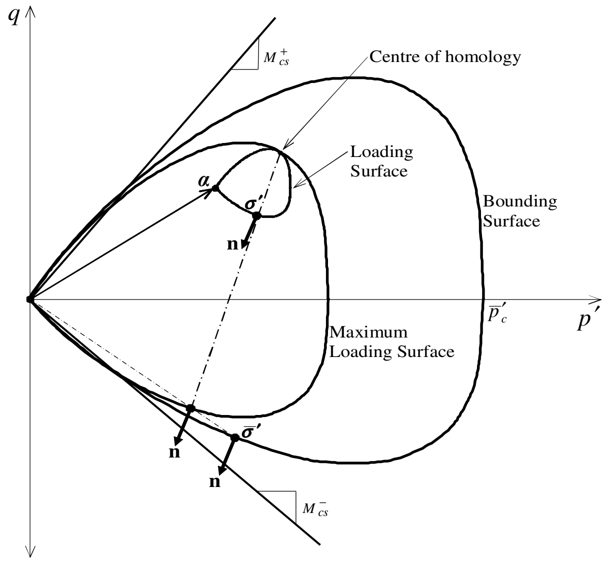

Figure 2. Illustration of mapping rule and the loading surface for cyclic loading

The loading history of the soil is captured through the stress reversal points and the corresponding maximum loading surfaces. In general, the loading surface (f) takes the form

$$f(\hat{p}', \hat{q}, \hat{p}'_c) = \left(\frac{\hat{q}}{M_{cs}\hat{p}'}\right)^N - \frac{\ln(\hat{p}'_c/\hat{p}')}{\ln R} = 0 \qquad [10]$$

where $\hat{p}' = p' - \alpha_p$, $\hat{q} = q - \alpha_q$, $\hat{p}'_c = p'_c - \alpha_p$, $\boldsymbol{\alpha} = [\alpha_p, \alpha_q]^T$ is the kinematic hardening vector controlling the position of the loading surface, and $\hat{p}'_c$ is the isotropic hardening parameter controlling the size of the loading surface. $\boldsymbol{\alpha}$ is determined by enforcing the constraint that the loading surface must be tangent to the local bounding surface at the centre of homology and pass through the current stress state $\boldsymbol{\sigma}'$. The unit normal vector at the image point defining the direction of loading is given using the general equation

$$\mathbf{n} = \frac{\partial f/\partial\boldsymbol{\sigma}'}{\|\partial f/\partial\boldsymbol{\sigma}'\|} = \frac{\partial F/\partial\bar{\boldsymbol{\sigma}}'}{\|\partial F/\partial\bar{\boldsymbol{\sigma}}'\|} \qquad [11]$$

3.3 Critical state and isotropic compression lines

The critical state (CS) is an ultimate condition towards which all states approach with increasing deviatoric shear strain. The critical state line (CSL) for unsaturated soils is expressed using

$$\upsilon_{cs} = \Gamma(s) - \lambda(s)\ln(p'_{cs}) \quad [12]$$

where $\Gamma(s)$ is specific volume at a reference mean effective stress of p' = 1kPa, $\lambda(s)$ is slope of the CSL on $\upsilon \sim \ln p'$ plane, υ_{cs} and p'_{cs} are the specific volume and mean effective stress at the critical state, respectively.

Implicit in the present investigation is the existence of a limiting isotropic compression line (LICL) located at a constant shift along the κ line from the CSL in the $\upsilon \sim \ln p'$ plane. The equation for the isotropic compression line is given by

$$\upsilon_{LICL} = N(s) - \lambda(s)\ln(\bar{p}'_c) \quad [13]$$

in which υ_{LICL} is the specific volumes on the LICL and $N(s)$ is intercept of the LICL at the reference mean effective stress of $p' = 1\,kPa$.

3.4 Plastic Potential

The plastic potential ($g=0$) defines the ratio between the incremental plastic volumetric strain and the incremental plastic shear strain. The stress-dilatancy relationship adopted in the current formulation is

$$d = \bar{\bar{t}} A\left(M_{cs} - \frac{q}{p'}\right) \quad [14]$$

where d is the dilatancy, A is a material constant dependant on the mechanism and amount of energy dissipation. The expression for the plastic potential (g) is then obtained by integrating [20] with respect to p and q as

$$g(\boldsymbol{\sigma}, p_o, \bar{p}_t) = \bar{\bar{t}}\left[q + \frac{AM_{cs}(p-\bar{p}_t)}{A-1}\left[\left(\frac{p-\bar{p}_t}{p_o-\bar{p}_t}\right)^{A-1} - 1\right]\right] \quad \text{for} A \neq 1 \quad [15]$$

$$g(\boldsymbol{\sigma}, p_o, \bar{p}_t) = \bar{\bar{t}}\left[q + M_{cs}(p-\bar{p}_t)\ln(\frac{p-\bar{p}_t}{p_o-\bar{p}_t})\right] \quad \text{for} A = 1$$

where p_o is the variable controlling the size of the plastic potential. A typical shape of the plastic potential is shown in Figure 3. Notice that two families of curves are identified: M_{cs}^{+} for compressive loading ($\bar{q} > 0$) and M_{cs}^{-} for extensive loading ($\bar{q} < 0$).

The direction of plastic flow is therefore defined as

$$\mathbf{m} = \frac{\partial g / \partial \boldsymbol{\sigma}'}{\left\| \partial g / \partial \boldsymbol{\sigma}' \right\|} \quad [16]$$

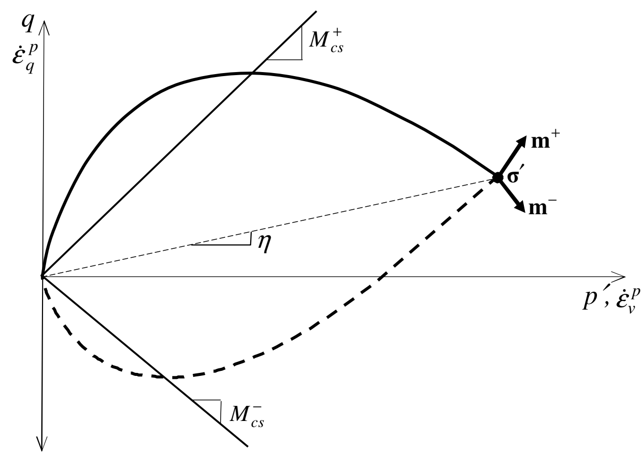

Figure 3. Typical shape of the plastic potential for compression and extension loadings in the q ~ p plane.

In this case, the sign of $\bar{\bar{t}}$ which controls the direction of plastic flow in the deviatoric plane is determined based on the relative positions of the stress point ($\boldsymbol{\sigma}'$) and its image point ($\bar{\boldsymbol{\sigma}}'$). The sign of $\bar{\bar{t}}$ is determined using $\bar{\bar{t}} = +1$ for $\left|\bar{\theta}_\sigma - \theta_\sigma\right| > 0.5\pi$ and $\bar{\bar{t}} = -1$ for $\left|\bar{\theta}_\sigma - \theta_\sigma\right| < 0.5\pi$, where θ_σ is the angle, measured clock-wise, from a given reference axis to the stress point in the deviatoric plane. For example, if the z-axis is taken as the reference axis,

$\theta_\sigma = \tan^{-1}\left[\sqrt{3}(\sigma'_y - \sigma'_x) \Big/ (2\sigma'_z - \sigma'_y - \sigma'_x)\right] + 2\pi$ for $\sigma'_z \geq 0$ and $\theta_\sigma = \tan^{-1}\left[\sqrt{3}(\sigma_y - \sigma_x) \Big/ (2\sigma_z - \sigma_y - \sigma_x)\right] + \pi$ for $\sigma'_z < 0$. $\bar{\theta}_\sigma$ is defined similar to θ_σ using the image stress point.

3.5 Hardening Modulus

Following the usual approach in bounding surface plasticity, the hardening modulus h is divided into two components

$$h = h_b + h_f \tag{17}$$

where h_b is the plastic modulus at $\bar{\boldsymbol{\sigma}}'$ on the bounding surface, and h_f is some arbitrary modulus at $\boldsymbol{\sigma}'$, defined as a function of the distance between $\bar{\boldsymbol{\sigma}}'$ and $\boldsymbol{\sigma}'$. h_b is determined by imposing the consistency condition at the bounding surface and incorporating the hardening effects of plastic volumetric strain and matric suction. The consistency condition for unsaturated soils is written as

$$\begin{aligned}\dot{F} &= \left(\frac{\partial F}{\partial \boldsymbol{\sigma}'}\right)^{\mathrm{T}} \dot{\boldsymbol{\sigma}}' + \frac{\partial F}{\partial \bar{p}'_c}\left(\frac{\partial \bar{p}'_c}{\partial \varepsilon_v^p}\dot{\varepsilon}_v^{\mathrm{p}} + \frac{\partial \bar{p}'_c}{\partial s}\dot{s}\right) = \\ &\left(\frac{\partial F}{\partial \boldsymbol{\sigma}'}\right)^{\mathrm{T}} \dot{\boldsymbol{\sigma}}' + \frac{\partial F}{\partial \bar{p}'_c}\left(\frac{\partial \bar{p}'_c}{\partial \varepsilon_v^p} + \frac{\partial \bar{p}'_c}{\partial s}\frac{\dot{s}}{\dot{\varepsilon}_v^{\mathrm{p}}}\right)\dot{\varepsilon}_v^{\mathrm{p}} = 0\end{aligned} \tag{18}$$

The plastic deformation of the solid skeleton is obtained from the existence of solid skeleton is obtained from the existence of plastic potential:

$$\dot{\boldsymbol{\varepsilon}}^p = \dot{\Lambda}\frac{\partial g}{\partial \boldsymbol{\sigma}} = \dot{\Lambda}\frac{\partial g}{\partial \boldsymbol{\sigma}'} \tag{19}$$

In which $\dot{\Lambda}$ is the plastic multiplier. Substituting the plastic flow rule [19], equation [18] is simplified to

$$\dot{F} = \mathbf{n}^{\mathrm{T}}\dot{\boldsymbol{\sigma}}' - \dot{\Lambda}h_b = 0 \tag{20}$$

which implies the hardening modulus h_b at the bounding surface for unsaturated soils is

$$h_b = -\frac{\partial F}{\partial \bar{p}'_c}\left(\frac{\partial \bar{p}'_c}{\partial \varepsilon_v^{\mathrm{p}}} + \frac{\partial \bar{p}'_c}{\partial s}\frac{\dot{s}}{\dot{\varepsilon}_v^{\mathrm{p}}}\right)\frac{m_p}{\left\|\partial F / \partial \bar{\boldsymbol{\sigma}}'\right\|} \tag{21}$$

The modulus h_f is defined such that it is zero on the bounding surface and infinity at the point of stress reversal. Following Khalili et al (2005) and Russell and Khalili (2006), h_f for unsaturated soils is taken as

$$h_f = \tilde{t}\left(\frac{\partial \bar{p}'_c}{\partial \varepsilon_v^{\mathrm{p}}} + \frac{\partial \bar{p}'_c}{\partial s}\frac{\dot{s}}{\dot{\varepsilon}_v^{\mathrm{p}}}\right)\frac{p'}{\bar{p}'_c}\left[\frac{\bar{p}'_c}{\hat{p}'_c} - 1\right]k_m(\eta_p - \eta) \tag{22}$$

where $\bar{p}'_c$ and $\hat{p}'_c$ define the sizes of the bounding and loading surfaces, respectively, $\eta = q / p'$ is the stress ratio, η_p is the slope of the peak strength line in the $q \sim p'$ plane, and k_m is a material parameter controlling the steepness of the response in the $q \sim \varepsilon_q$ plane.

3.6 Suction Hardening

The general effect of suction is to increase the effective stress and hardens the soil response. The increase in the soil stiffness leads to an increase in both the intercept $N(s)$ and slope $\lambda(s)$ of the isotropic compression line, which will have a net effect of increasing the size of the bounding surface ($\bar{p}'_c$). There are two approaches for incorporating the hardening effect of suction; a coupled influence where suction has a multiplicative effect to the plastic volumetric hardening; or a decoupled influence where suction has an additive effect on the hardening parameter (Loret and Khalili, 2000; Russell and Khalili, 2006). In the formulation presented here, the approach proposed by Loret and Khalili (2002) which considers a coupled effect of suction hardening is adopted. For the coupled approach, the general expression for the hardening rule is given by

$$\bar{p}'_c\left(\varepsilon_v^{\mathrm{p}}, s\right) = \bar{p}'_{ci}\gamma(s)\exp\left(\frac{v_i \Delta\varepsilon_v^{\mathrm{p}}}{\lambda(s) - \kappa}\right) \tag{23}$$

where v_i is the initial specific volume, $\bar{p}'_{c,i}$ is the initial value of the hardening parameter, $\Delta\varepsilon_v^{\mathrm{p}}$ is the increment of plastic volumetric strain, $\gamma(s)$ is a function representing the coupled effect of suction hardening and can be determined considering the shift in the limiting isotropic compression line (LICL) due to suction change. Loret and Khalili (2002) derived the following expression for $\gamma(s)$

$$\gamma(s) = \exp\left(\frac{N(s) - N(s_i)}{(\lambda(s) - \kappa)} - \frac{(\lambda(s) - \lambda(s_i))}{(\lambda(s) - \kappa)}\ln(\bar{p}'_{ci})\right) \tag{24}$$

in which $N(s_i)$ and $\lambda(s_i)$ are intercept and slope of the LICL at the initial suction s_i, while $N(s)$ and $\lambda(s)$ are intercept and slope of the LICL at the final suction s.

3.7 Elasto-Plastic Stress-Strain Relations

Solving for the plastic multiplier $\dot{\Lambda}$ from the consistency condition [18]

$$\dot{\Lambda} = \frac{1}{h_b}\mathbf{n}^{\mathrm{T}}\dot{\bar{\boldsymbol{\sigma}}}' \qquad [25]$$

where $\mathbf{n}$ is the unit vector normal to the bounding surface at the image stress point and h_b is the plastic modulus at the image point $\bar{\boldsymbol{\sigma}}'$ on the bounding surface. Recalling the basic assumption of bounding surface theory, the equivalent form of the plastic multiplier at the current stress state $\boldsymbol{\sigma}'$ can be written as

$$\dot{\Lambda} = \frac{1}{h_b}\mathbf{n}^{\mathrm{T}}\dot{\bar{\boldsymbol{\sigma}}}' = \frac{1}{h}\mathbf{n}^{\mathrm{T}}\dot{\boldsymbol{\sigma}}' \qquad [26]$$

where h is the plastic modulus at the current stress point. Expressing elastic stress-strain relationship

$$\dot{\boldsymbol{\sigma}}' = \mathbf{D}^{\mathrm{e}}\dot{\boldsymbol{\varepsilon}}^{\mathrm{e}} = \mathbf{D}^{\mathrm{e}}(\dot{\boldsymbol{\varepsilon}} - \dot{\boldsymbol{\varepsilon}}^{\mathrm{p}}) = \mathbf{D}^{\mathrm{e}}(\dot{\boldsymbol{\varepsilon}} - \dot{\Lambda}\mathbf{m}) \qquad [27]$$

Where $\mathbf{D}^{\mathrm{e}}$ is the elastic stiffness matrix of the solid skeleton. Combining [27] with [26] and the consistency condition yields

$$\dot{\Lambda} = \frac{\mathbf{n}^{\mathrm{T}}\mathbf{D}^{\mathrm{e}}\dot{\boldsymbol{\varepsilon}}}{h + \mathbf{n}^{\mathrm{T}}\mathbf{D}^{\mathrm{e}}\mathbf{m}} \qquad [28]$$

where $\mathbf{m}$ is the unit direction of plastic flow at $\dot{\boldsymbol{\sigma}}'$.
Therefore, the elasto-plastic stress-strain relation for unsaturated soils is expressed as

$$\dot{\boldsymbol{\sigma}}' = \left(\mathbf{D}^{\mathrm{e}} - \frac{\mathbf{D}^{\mathrm{e}}\mathbf{m}\mathbf{n}^{\mathrm{T}}\mathbf{D}^{\mathrm{e}}}{h + \mathbf{n}^{\mathrm{T}}\mathbf{D}^{\mathrm{e}}\mathbf{m}}\right)\dot{\boldsymbol{\varepsilon}} = \mathbf{D}^{\mathrm{ep}}\dot{\boldsymbol{\varepsilon}} \qquad [29]$$

where $\mathbf{D}^{\mathrm{ep}}$ is the standard elasto-plastic stress-strain matrix of the of the soil.

4 MODEL VALIDATION

To demonstrate the application of the fully coupled model, several loading conditions involving mechanical and hydraulic hysteresis should be analysed. Due to space limitation, the model simulations are compared with only one of the experimental data available in the literature among the others. The following case is chosen to examine one of the main contributions of this work which is the incorporation of hydraulic hysteresis into mechanical modelling of unsaturated soil mechanics.

4.1 Drying-Wetting Cycle Tests on White Clay

Fleureau *et al* (1993) carried out experimental research to investigate the response of unsaturated clayey soils subjected to drying-wetting paths at constant net stress. The tests were conducted on initially saturated slurries that were preconsolidated in an oedometer. The applied load path involved first increasing suction to a specified value followed by decrease in suction to its initial value while the net stress was kept constant. Suction was controlled by keeping the pore air pressure zero (at atmospheric pressure) and varying the pore water pressure. The stress paths along with some of the numerical simulations obtained using the proposed model in comparison with the experimental data are shown in Figures 4 and 5.

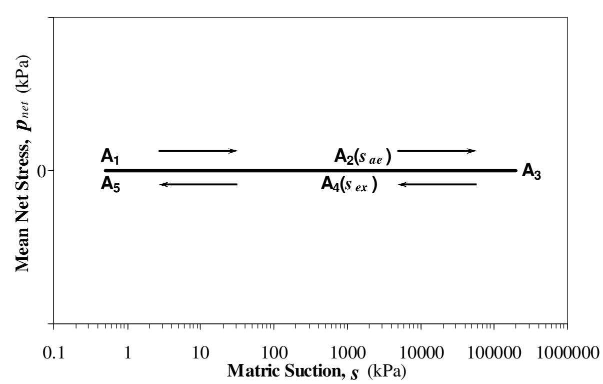

Figure 4. Stress path for the drying- wetting cycle test on white clay.

The material parameters used in the simulations were calibrated from the experimental data reported by Fleureau *et al* (1993). The air entry and air expulsion values of s_{ae} = 1600 kPa and s_{ex} = 1200 kPa were obtained from the soil water characteristic curve. Initial void ratio of the sample was e = 1.96 and the initial preconsolidation stress of the fully saturated sample was $\bar{p}'_c$ = 10 kPa. Material parameters defining the isotropic compression line of the saturated state were $\lambda(0) = 0.191$ and $N(0) = 3.214$. For unsaturated states, variation of these parameters with suction were back calculated by applying the suction hardening rule proposed by Loret and Khalili (2000) on the values of the preconsolidation stress. Other model parameters used in the analysis were $\kappa = 0.014$, $\nu = 0.3$, $M_{cs} = 0.85$, $N = 2.0$, $R = 2.0$, $A = 1.0$, $\zeta = 0.5$, $\xi = 0$ and $k_m = 1.0$.

Figure 4 shows the drying-wetting path (A_1-A_2-A_3-A_4-A_5) in the mean net stress - suction ($p_{net} \sim s$) plane. For instance, the resulting changes in the specific volume are shown in Figures 5. It can be seen form this figure that the model simulations match the experimental data very well for both drying and wetting paths.

Notice that for the portion of the drying path below the air entry suction (A_1-A_2), the soil behaviour is saturated with the increase in suction resulting in an equal increase of the effective stress leading to compression of the sample. As is shown in Figures 5, initial part of this path corresponds to elastic deformation until the effective stress equals the preconsolidation (yield) stress at A_y, after which plastic deformation occurs until the air entry suction is reached. This stage (A_y-A_2) is associated with equal increments of the mean effective and preconsolidation stresses. The increase in the yield stress is solely due to the hardening effect of plastic volumetric strain.

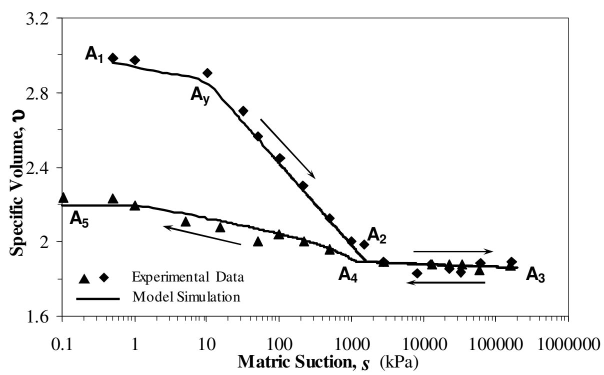

Figure 5. Comparison of model simulation and experimental data for the drying-wetting cycle test on white clay, $\upsilon \sim s$ plot.

Once the air entry suction is reached, the soil becomes unsaturated with the change in effective stress becoming less than the change in suction, while the increase in the preconsolidation stress becoming larger due to contribution of suction hardening. At this stage, since the increase in the mean effective stress is less than the increase in the yield stress, the deformation after the air entry value (A_2-A_3) is inside the bounding surface. In fact the volumetric compression of the soil in this region is much smaller for the unsaturated range due to progressively smaller rate of increase in the effective stress.

The volume change behaviour during the first stage of the wetting path (A_3-A_4) is the exact reverse of the behaviour in the unsaturated range for the drying path (A_2-A_3). A reduction in the suction leads to a decrease in both the effective stress and the preconsolidation stress with the reduction in the preconsolidation stress being greater than the reduction in the effective stress. Since the mean effective stress is less than the preconsolidation stress, the reduction in suction results in predominantly elastic swelling of the sample. On the other hand, hardening effect of suction vanishes and the preconsolidation stress becomes constant when suction is below the air expulsion value (A_4-A_5). This leads to further swelling as the effective stress continues to decrease within the bounding surface with reduction in suction.

The proposed model is also able to capture the hydraulic hysteresis between the drying and wetting stages of the soil water characteristic curve. This was possible by using two different values of s_e in determination of the effective stress parameter. The air entry suction ($s_e = s_{ae}$) is used for the drying path, while the air expulsion ($s_e = s_{ex}$) suction is used for the wetting path. This feature was not captured in the simulations of Loret and Khalili (2000) since they have used the same air entry and air expulsion values for the drying and wetting paths. In general, the above results confirm capability of the proposed model to describe the basic behaviour of unsaturated soils for drying-wetting load cycle.

5 CONCLUSION

A fully coupled elasto-plastic constitutive model is presented for unsaturated soils including hydraulic and mechanical hystereses. The model is formulated incrementally using the effective stress principle with the effective stress parameter defined as a function of suction. The elastic-plastic deformation behaviour is captured using bounding surface plasticity. Effect of suction on plastic hardening is taken in to account through definition of the isotropic compression line. A single set of material parameters is introduced for the complete characterization of the coupled constitutive model. Model simulation is compared with experimental data. Good agreement is obtained between the simulation results and the test data in all the cases considered.

REFERENCES

Alonso EE., Yang DQ., Lloret A. and Gens A. 1995. Experimental behaviour of highly expansive double-structure clay. *Proceedings of the 1995 1st International Conference on Unsaturated Soils.* Paris, France: v 1, p11

Bishop AW., 1959. The principle of effective stress. *Teknisk Ukeblad*,106(39): 859–863.

Bishop AW and Blight GE. 1963. Some aspects of effective stress in saturated and partly saturated soils. *Géotechnique,* 13: 177–197.

Bishop A.W. and Donald I. B. 1961. The experimental study of partly saturated soil in triaxial apparatus. *Proc., 5th Int. Conf. SMFE*, Dunod, Paris: 13–21.

Buisson, MSR. & Wheeler, SJ. 2000. Inclusion of hydraulic hysteresis in a new elasto-plastic framework for unsaturated soils., In *Experimental evidence and theoretical approaches in unsaturated soils* (eds A. Tarantino and C. Mancuso), Rotterdam: Balkema, 109–119.

Dafalias YF, Herrmann LR. 1980. A Bounding surface soil plasticity model. *International Symposium on Soils under Cyclic and Transient Loading*, Swansea: 335-345.

Fleureau, JM., Kheirbeksaoud, S., Soemitro, R., and Taibi, S. 1993. Behavior of clayey soils on drying wetting paths. *Canadian Geotechnical Journal*, 30(2): 287-296.

Gallipoli G., Gens A., Sharma R., Vaunat J. 2003. An elasto-plastic model for unsaturated soil incorporating the effects of suction and degree of saturation on mechanical behaviour, *Geotechnique,* 53; 123–135.

Habte M.A. and Khalili N. 2006. A constitutive model for cyclic analysis of unsaturated soils. *4th Int. Conf. Unsaturated Soils*, UNSAT 2006, April 2-5, Carefree, Arizona, 1920-1931.

Hassanizadeh SM, Gray WG. 1990. Mechanics and thermodynamics of multiphase flow in porous-media including interphase boundaries. *Advances in Water Resources*, 13(4):169–186.

Houlsby GT. 1997. The work input to an unsaturated granular material, *Geotechnique*, 47(1): 193-196.

Jommi C. 2000. Remarks on the constitutive modelling of unsaturated soils, Experimental Evidence and Theoretical Approaches in Unsaturated Soils, *Proc. of Int. Workshop on Unsaturated Soil* (Tarantino A and Mancuso C, eds), Balkema, Rotterdam, 139-153.

Khalili N and Khabbaz MH. 1998. A unique relationship for χ for the determination of the shear strength of unsaturated soils, *Géotechnique* 48, 2:1-7.

Khalili N, Geiser F, and Blight GE. 2004. Effective stress in unsaturated soils: Review with New Evidence, *International Journal of Geomechanics*, 4(2): 115-126.

Khalili N, Habte MA, and Valliappan S. 2005. A bounding surface plasticity model for cyclic loading of granular soils, *International Journal for Numerical Methods in Engineering*, 63(14): 1939-1960.

Khalili, N., and Zargarbashi, S. 2009. Hydraulic hysteresis and effective stress in unsaturated soils, *Geotechnique*, under review.

Laloui L., Klubertanz, G., and Vulliet L. 2003. Solid-liquid-air coupling in multiphase porous media, *International Journal for Numerical and Analytical Methods in Geomechanics*, 27(3): 183-206.

Loret B and Khalili N. 2000. A three-phase model for unsaturated soils, *Int. J. Numer. Anal. Meth. Geomech.*, 24: 893–927.

Loret B and Khalili N. 2002. An effective stress elastic-plastic model for unsaturated porous media, *Mechanics of materials*, 34:97–116.

Muraleetharan KK, Wei CF. 1999. Dynamic behaviour of unsaturated porous media: governing equations using the theory of mixtures with interfaces (TMI), *International Journal for Numerical and Analytical Methods in Geomechanics*, 23(13):1579–1608.

Russell, A. R., and Khalili, N. 2006. A unified bounding surface plasticity model for unsaturated soils, *International Journal for Numerical and Analytical Methods in Geomechanics*, 30(3): 181-212.

Sun DA, Sheng D.C., Cui H. B. and Sloan S.W. 2007a. A density-dependent elastoplastic hydro-mechanical model for unsaturated compacted soils, *Int. J. Numer. Anal. Meth. Geomech*, 31:1257–1279

Sun DA, Sheng D and Sloan SW. 2007b. Elastoplastic modelling of hydraulic and stress-strain behaviour of unsatuarated soil, *Mechanics of Materials*, 39(3): 212-221.

Tamagnini R. 2004. An extended Cam-clay model for unsaturated soils with hydraulic hysteresis, *Geotechnique*, 54: 223–228

Vaunat, J, Romero E and Jommi C. 2000. An elastoplastic hydromechanical model for unsaturated soils, *Experimental Evidence and Theoretical Approaches in Unsaturated Soils, Proc. of Int. Workshop on Unsaturated Soil (Tarantino A and Mancuso C, eds),* Balkema, Rotterdam, 121-138.

Wheeler SJ, Sharma RS and Buisson MSR. 2003. Coupling of hydraulic hysteresis and stress-strain behaviour in unsaturated soils, *Geotechnique*, 53(1): 41-54.

Zerhouni 1991. Application des réseaux de Petri continus à l'analyse dynamique des systèmes de production- ThOse do Doctorat do l'INP Grenoble, France